

## Article

# pH-Sensitive Fluorescence Emission of Boron/Nitrogen Co-Doped Carbon Quantum Dots

Oguzhan Ustun<sup>1</sup>, Sugra Naz Karadag<sup>2</sup>, Hayrunnisa Mazlumoglu<sup>3</sup>, Asli Yilmaz<sup>2,\*</sup>  and Mehmet Yilmaz<sup>1,3,\*</sup> <sup>1</sup> Department of Nanoscience and Nanoengineering, Ataturk University, Erzurum 25240, Turkey<sup>2</sup> Department of Molecular Biology and Genetics, Ataturk University, Erzurum 25240, Turkey<sup>3</sup> Department of Chemical Engineering, Ataturk University, Erzurum 25240, Turkey

\* Correspondence: asliozdilek@gmail.com (A.Y.); nano.yilmaz@gmail.com (M.Y.)

**Abstract:** Carbon quantum dots (CQDs) with their strong photoluminescence (PL) activity, high biocompatibility, robust stability, low cytotoxicity, and flexible surface structures have been employed in many fields including chemical sensing, biosensing, photocatalyst, energy storage, and biomedical applications. Of note, CQDs present an intrinsic pH-sensitive PL nature indicating their intense potential for pH-mediated sensing and imaging. Despite the numerous studies performed in the last two decades, the pH-sensitive PL mechanism of CQDs is still under debate and must be clarified to overcome the limitations in practical applications. Therefore, in this report, we performed a systematical study to determine the pH-sensitive PL nature of boron/nitrogen co-doped CQDs (B/N CQDs). In the first part, B/N CQDs with a strong blue emission were fabricated via a hydrothermal synthesis procedure. B/N-CQDs showed a strong blue PL emission with high quantum yield and excitation-dependent nature. Under the low pH conditions (pH 3), B/N-CQDs exhibited a robust green fluorescence emission with a significant red-shift (48 nm) and the loss of the excitation-dependent nature. The change in PL nature originated from the protonation of surface groups, a decrease in negative surface charge (from  $-20.6$  to  $-1.23$  eV), and finally, aggregation of the nanostructure (the size of CQDs from 4.8 to 7.5 nm). However, in the case of alkaline conditions, the deprotonation surface groups significantly enhanced the surface charge and led to the emergence of a negative 'protective shell' with a zeta potential of  $-71.3$  eV. In a high pH medium (pH 13), PL spectra showed the loss of excitation-dependent features and a red-shift (35 nm) in emission peak maxima with lower intensity. This report provides significant progress in the clarification of the pH-sensitive PL mechanism of CQDs. We envision that the proposed CQDs would provide unique opportunities in the fabrication of novel pH sensor systems and fluorescence imaging where a wide range of pH sensitivity is required.

**Keywords:** pH-sensitive fluorescence; co-doped carbon quantum dots; aggregation-induced emission; excitation-dependent emission; hydrothermal synthesis



**Citation:** Ustun, O.; Karadag, S.N.; Mazlumoglu, H.; Yilmaz, A.; Yilmaz, M. pH-Sensitive Fluorescence Emission of Boron/Nitrogen Co-Doped Carbon Quantum Dots. *Coatings* **2023**, *13*, 456. <https://doi.org/10.3390/coatings13020456>

Academic Editors: Csaba Balázsi and Rafael L. Quirino

Received: 19 December 2022

Revised: 31 January 2023

Accepted: 15 February 2023

Published: 17 February 2023



**Copyright:** © 2023 by the authors. Licensee MDPI, Basel, Switzerland. This article is an open access article distributed under the terms and conditions of the Creative Commons Attribution (CC BY) license (<https://creativecommons.org/licenses/by/4.0/>).

## 1. Introduction

For the last two decades, carbon quantum dots (CQDs) as a zero-dimensional carbon nanomaterial, which have sizes lower than 10 nm have gained intense interest due to their impressive advantages, including their widespread source of precursors, small sizes, strong photoluminescence (PL), high biocompatibility and photostability, low cytotoxicity and, flexible surface structures [1–4]. With their unique properties, CQDs have been employed in various applications such as chemical sensing, biosensing, photocatalysts, energy storage, and biomedical applications [5–9]. Unlike other carbon-based nanomaterials, CQDs possess a graphitic core composed of  $sp^2/sp^3$  hybrid with numerous functional groups, which consist of primarily oxygen-related groups and post-modified chemical groups on the surface [10–12]. For the fabrication of CQDs, hydrothermal/solvothermal, microwave

irradiation, arc discharge, laser ablation, and electrochemical oxidation methods have been employed by utilizing various precursors under different experimental conditions [13].

The PL characteristics of CQDs could be manipulated by simply tuning the environmental conditions such as pH, ionic strength, etc. [10]. This unique phenomenon enables their utilization as pH sensors and imaging. The determination of pH is essential in various fields of biomedicine, agriculture, and industry. The monitoring of pH with novel, sensitive, and robust systems might provide unique advantages in real-world applications such as the diagnosis of diseases, environmental control, quality of food and beverage products, and so on [14,15]. CQDs as pH-sensitive nanoproboscopes eliminate the limitations of organic dyes and inorganic QDs in terms of toxicity, PL quenching, and background autofluorescence [16,17]. Interestingly, CQDs with a pH-sensitive nature are quite different in terms of synthesis procedure, precursors, chemical structure, and morphology [14,15]. In the last two decades, many experimental procedures have been proposed for the fabrication of pH-sensitive CQDs. The work by Liu et al. showed that CQDs prepared from candle soot with multicolor fluorescence showed increased and then decreased PL intensity when pH was tuned from 3 to 13 [18]. Similarly, Lu et al. prepared CQDs with a white fluorescent emission by a hydrothermal method and detected that the PL intensity gradually decreased when the pH ranged from 0 to 14 [19]. Zhu et al. proposed N-doped CQDs which were fabricated through a solvothermal method for the detection of pH monitoring in cells using fluorescence imaging [20]. Similarly, Fan et al. showed the employment of pH-responsive CQDs through green-blue-violet fluorescence transformation for *in vitro* cell imaging [21]. So far, several mechanisms have been proposed to clarify the pH-sensitive PL characteristics of CQDs. In most cases, the researchers attributed the change in the PL spectrum and intensity of the material to the deprotonation and protonation of acidic and basic surface groups such as carboxyl, hydroxyl, and carbonyl [10]. These groups could mainly govern the transition processes and resulting PL nature. For instance, Li et al. prepared highly fluorescent CQDs using tetrahydrofuran as a precursor and observed a linear decrease in PL intensity due to the reversible protonation and deprotonation of surface functional groups [22]. In another study, CQDs with PL maxima peak at 630 nm was shifted to 590 nm with lower intensity when the pH was increased from 7 to 14 [23]. The authors claimed that the increase in pH led to the deprotonation of carboxyl and hydroxyl groups and resulted in a change in PL characteristics. In addition to the deprotonation/protonation of surface groups, some researchers have proposed that the pH sensitivity of CQDs might originate from the pH-induced aggregation. For example, Sun et al. observed that the decrease in pH created a significant decrease in zeta potentials and induced aggregation and resulted in quenching [24]. In a similar vein, Ye et al. observed that the pH under alkaline conditions formed intermolecular hydrogen bonds and led to aggregation and finally PL quenching [25].

Despite numerous studies in the literature, the pH sensitivity of CQDs over PL characteristics is still controversial and this issue dramatically limits their employment in practical applications. Therefore, it is unquestionable that further experimental and theoretical studies are demanded to clarify and interpret the pH-sensitive PL nature of CQDs. Within this context, in this study, we have investigated PL characteristics of boron/nitrogen co-doped CQDs (B/N CQDs) in different pH conditions. Just like our earlier study [3], B/N CQDs with strong blue emission were synthesized through a hydrothermal procedure using sodium borohydride and dopamine as precursors. We examined the alterations of the chemical and morphological structure of the material under various pH environments via some spectroscopic and imaging techniques. In an acidic environment, the aggregation of CQDs led to the formation of larger nanoparticles and the emergence of green fluorescence emissions. However, under alkaline conditions, a negative “protective shell” was formed on the surface of the material due to the deprotonation of oxygen-related groups. This study clarifies the pH-sensitive PL mechanism of CQDs in detail through various analyses. We strongly believe that the findings of this report should pave the way for potential appli-

cations of CQDs, especially in biomedical applications such as monitoring pH fluctuations of single living cells and the whole organism.

## 2. Materials and Methods

### 2.1. Synthesis of B/N-CQDs via Hydrothermal Synthesis

B/N-CQDs were synthesized through a hydrothermal method similar to our earlier report [3]. Briefly, 38 mg of dopamine hydrochloride (98%, Sigma-Aldrich, Taufkirchen, Germany) and 7.6 mg of sodium borohydride ( $\text{NaBH}_4$ , 98%, Sigma-Aldrich Taufkirchen, Germany) were dissolved in 10 mL distilled water with a conductivity of  $0.05 \mu\text{S}/\text{cm}$ . After 10 min of magnetic stirring, the clear solution was transferred into a 40 mL Teflon-lined stainless-steel reactor. The synthesis was performed in an oven at  $180^\circ\text{C}$  for 12 h. To terminate the reaction, the reactor was taken and left at ambient temperature to cool to room temperature. For the purification, firstly, the colloidal suspension was centrifuged at 14,800 rpm for 20 min to remove large aggregates. Then, the CQDs were dialyzed to remove unreacted impurities using a dialysis membrane (1 kDa MW cut-off) for 24 h. The pH of as-prepared B/N-CQDs was adjusted by adding a proper amount of HCl (1 M) and NaOH (1 M) aqueous solutions. Special care was paid to determine the exact pH value. After the addition of HCl or NaOH, the measurements were repeated three times in 3 min time intervals for clarification. For the calculation of the fluorescence quantum yield (QY) of B/N-CQDs, quinine sulfate was employed as a standard similar to earlier reports [26,27].

### 2.2. Characterization of B/N-CQDs

The absorption spectra of CQDs were collected from a Shimadzu UV-vis spectrophotometer (Shimadzu, UV-1800, Kyoto, Japan). An Agilent Cary Eclipse fluorescence spectrophotometer (Santa Clara, CA, USA) was employed to evaluate the fluorescence characteristics. An X-ray photoelectron spectroscopy (XPS, Specs-Flex, Berlin, Germany) was used to determine the surface states of B/N-CQDs. The size and morphology were performed via a Hitachi HighTech HT7700 transmission electron microscope (TEM, Krefeld, Germany) operated at 120 kV. The surface charge of B/N-CQDs was measured with a Malvern Zetasizer Nano ZSP (Worcestershire, United Kingdom). The pH value of B/N-CQDs was adjusted through a Mettler Toledo pH meter (Columbus, OH, USA). All measurements were performed at room temperature.

## 3. Results and Discussions

In this study, we aimed to determine the pH-sensitive fluorescence activity of B/N-CQDs under acidic and alkaline conditions. The original pH of the pristine as-prepared CQDs was around 8.0 with a pale-yellow color (Figure 1b). Under this condition, B/N-CQDs exhibited strong blue fluorescence emission under a 365-nm UV lamp with excitation-dependent characteristics with a high QY of 24% by using quinine sulfate as a reference material (Figure 1b). The increased excitation wavelength from 300 nm to 420 nm led to a red-shift in the fluorescence maxima ranging from 407 to 473 nm. For the case of pristine CQDs, UV-vis absorption spectra (Figure 2a) showed a weak shoulder at around 220 nm assigned to the  $\pi\text{-}\pi^*$  transition band of aromatic C-C bonds and a prominent peak around 278 nm attributed to the  $n\text{-}\pi^*$  transition of oxygen-related groups [12,28]. In addition, a broad shoulder at around 384 nm indicated the presence of lower energy states due to N-related functional surface groups [27–29]. It seems that the surface groups of B/N-CQDs create trap states with different energy levels and resultant excitation-dependent nature [1,3]. The PL spectra, optical images, and UV-vis absorption spectra of B/N-CQDs at different pH values are summarized in Figures S1–S3. Moreover, the Raman and FT-IR spectra provided from our previous study [3] showed high content of defects and disorders as well as various hydrophilic groups indicating the carbonization of the precursors and optical and hydrophilic nature of resultant CQDs.

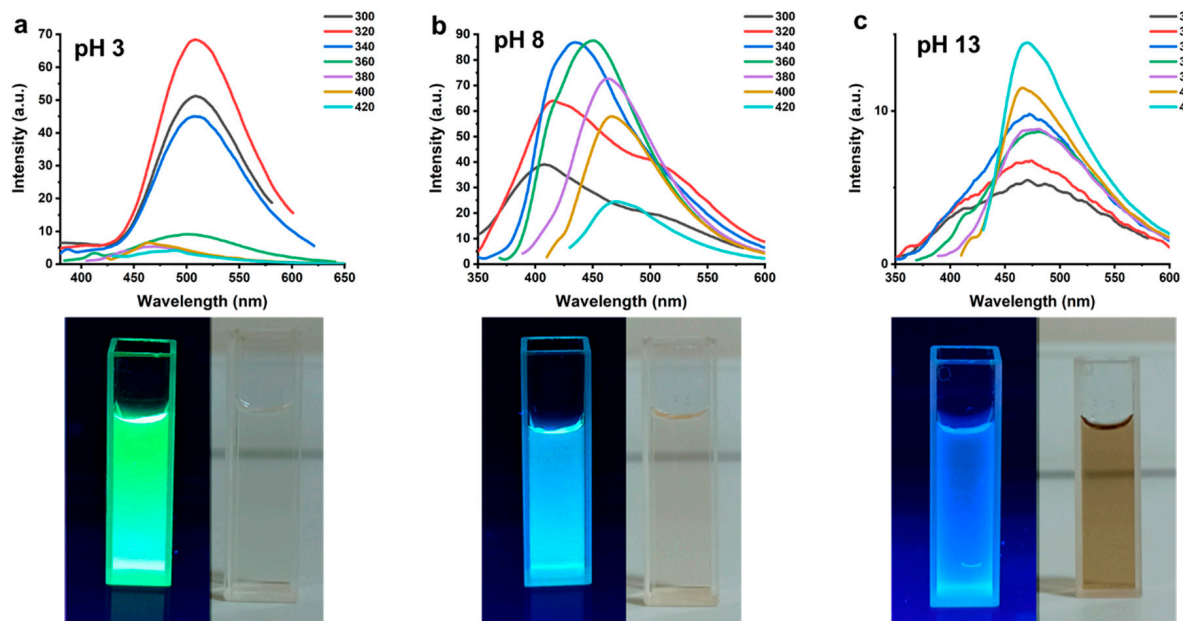


**Figure 1.** PL spectra of B/N-CQDs at pH values of 3 (a), 8 (b), and 13 (c) and their corresponding optical images under daylight and a 365-nm UV lamp.

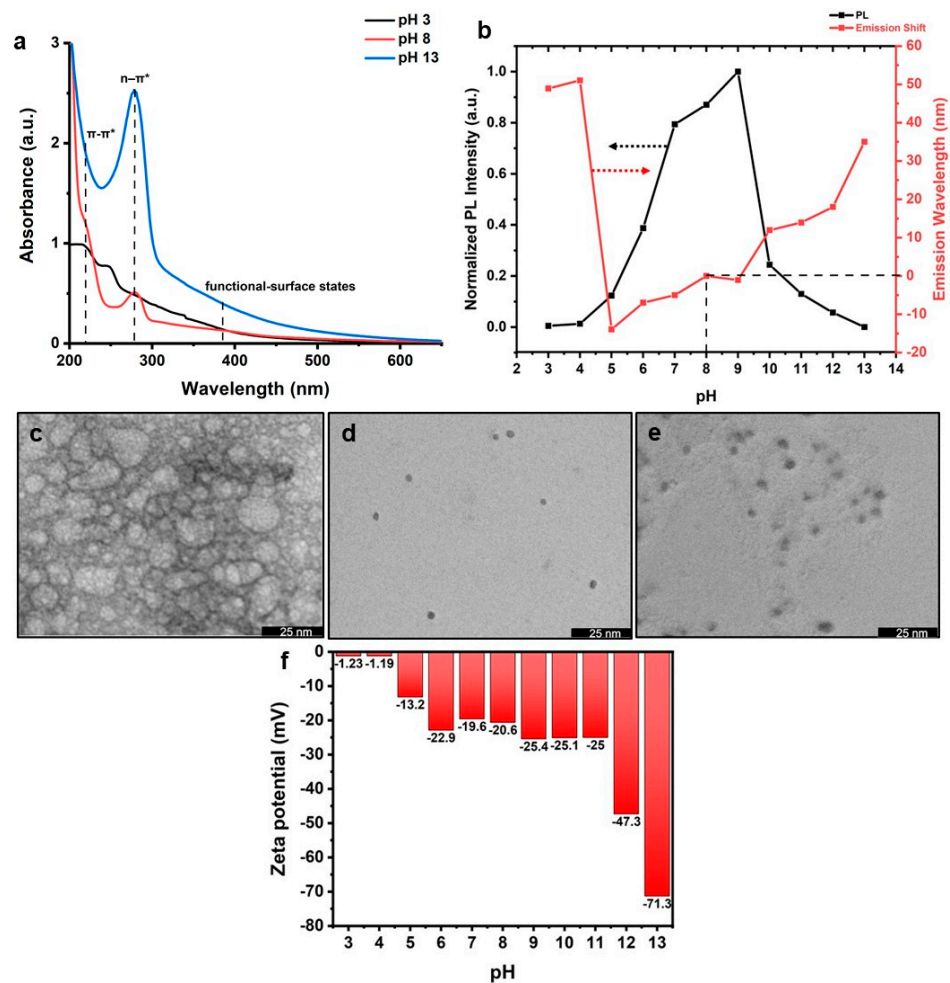


**Figure 2.** UV-vis spectra (a), PL intensity and the shift in emission maxima (ex. at 360 nm) (b), TEM images ((c–e) for pH of 3, 8, and 13, respectively), and Zeta potentials (f) of B/N-CQDs at different pH values.

The manipulation of the pH condition created dramatic changes in the PL properties of CQDs in terms of PL intensity, emission maxima, and excitation-dependent characteristics (Figures 1 and 2a,b). Under the acidic conditions (pH 3, Figure 1a), B/N-CQDs exhibited a strong green fluorescence emission due to the strong red-shift from 435 to 508 nm under a 340 nm excitation. However, the excitation-dependent nature was lost (Figure 1a) with lower fluorescence intensity (Figure 1a) in comparison to pristine pH (8) conditions. Under acidic conditions, the UV-vis absorption spectra (Figure 2a) indicated that oxygen-related groups disappeared, a new transition band appeared at 249 nm, and the  $\pi$ - $\pi^*$  transition peak showed a slight blue shift from 220 to 216 nm. Moreover, CQDs at pH 3 exhibited a long absorption tail from 260 to 550 nm. It was anticipated that all these optical changes governed the PL characteristics at lower pH values to some extent. Under the alkaline conditions, for CQDs at pH 13, the color of the solution under daylight was dark brown, and a faint blue fluorescence emission was observed compared with the pristine pH condition (Figure 1c). Similar to pH 3, PL spectra revealed that the excitation-dependent feature was lost, and the emission peak maxima were detected at around 470 nm with lower intensity for different excitation wavelengths. For the case of pH 13, the UV-vis absorption spectra (Figure 2a) showed that the  $\pi$ - $\pi^*$  transition band at around 220 nm, and a broad shoulder at around 384 nm due to N-related functional-surface groups were significantly enhanced due to the deprotonation surface groups.

On the other hand, the  $n$ - $\pi^*$  transition of oxygen-related groups at around 278 nm disappeared. This observation indicated that the PL properties of CQDs under acidic and alkaline conditions differ in line with the literature. In our case, we determined that in the surface state, the oxygen-containing groups in the outer shell have the dominant impact on the PL characteristics of the material [12]. Protonation and deprotonation of oxygen-related and heteroatom-derived groups in the structure lead to the emergence of different energy transitions and finally affect the PL spectra and intensity of the CQDs [10,30,31]. To evaluate the protonation and deprotonation of oxygen-related and heteroatom-derived groups, we measured the surface charges of CQDs at different pH values and summarized these values in Figure 2f. Under alkaline conditions, most of the surface groups were deprotonated. As a result, a negative “protective shell” was formed on the surface of the B/N-CQDs. The deprotonation of oxygen-related groups enhanced the electrostatic repulsion and formed isolated particles with high zeta potential, indicating the material’s high stability [22,32]. Whereas under acidic conditions, the zeta potential values reduced significantly (Figure 2f), showing the destruction of the protective shell and formation of new surface states. These phenomena may pave the way for pH-dependent aggregation, PL quenching, and a red-shift in emission maxima [10]. To clarify this issue, we collected many TEM images for CQDs at pH values of 3, 8 (pristine), and 13, and some representative ones are summarized in Figure 2c–e. For the case of pristine pH, B/N-CQDs showed a very narrow particle size distribution in the range of 3–7 nm with an average of 4.8 nm (Figure 2d). The CQDs are well-separated, indicating the material’s high stability due to their high zeta potential (−20.6 eV). Under alkaline conditions (Figure 2e), the nanostructures are still well-separated with a relatively high size distribution (4–9 nm) with an average of 6.1 nm. However, for the case of pH 3 (Figure 2c), B/N-CQDs were gathered into larger particles (about the average size of 7.5 nm) due to the lower zeta potential (−1.23 eV) and noncovalent molecular interactions, such as hydrogen bonds between the carboxyl groups [33]. The aggregation of CQDs led to the formation of larger nanoparticles and resulted in the narrowing of the band gap. This phenomenon may explain the emission of green fluorescence in an acidic environment [34].

To further examine the pH-sensitive fluorescence activity of B/N-CQDs under acidic and alkaline conditions, we performed a detailed XPS analysis to determine the chemical composition and surface groups at pH 3, 8, and 13. In the full spectra of XPS, four peaks at 192, 284, 400, and 532 eV were observed, corresponding to C-C/C=C, C-N, C-O, and C=O bonds, respectively (Figure S4). The elemental percentages of C/N/O/B were 81.6/0.93/15.9/1.55 for pH 3, 68.7/5.99/22.9/2.37 for pH 8 and 73.5/2.02/22.1/2.3 for

pH 13, respectively (Figure S4b). These data indicate that co-doping of the B and N in the structure of the CQDs was achieved, and the elemental content of the material can be manipulated significantly by tuning the pH. The high-resolution scans of the C1s, N1s, O1s, and B1s regions of B/N-CQDs are demonstrated in Figure 3. The core-level spectra of the C1s were convoluted to four characteristic peaks at 284.5, 285.6, 286.4, and 289.9 eV, corresponding to C-C/C=C, C-N, C-O, and C=O bonds, respectively. O1s band of CQDs can be divided into two prominent peaks at 531.6 and 532.5 eV, which can be assigned to C=O and C-O. The deconvolution of C1s and O1s showed that the presence of C-O and C=O is evidence for oxygen-related groups like carbonyl and carboxyl groups [35]. The N1s spectra present three distinct peaks at 398.7, 400.0, and 401.1 eV, which correspond to N-(C)<sub>3</sub> (graphitic), C=N-C (pyridinic), and N-H (pyrrolic), respectively [36,37]. The core level B1s spectrum was deconvoluted into four major peaks centered at 190.9, 191.8, 192.5, and 193.4 eV indicators of B-C, B-N/B-CO<sub>2</sub>, C-B-N, and B-O bonds, respectively [38]. We also performed detailed analyses on XPS spectra to determine the change in the chemical structure of CQDs in different pH conditions. As pH was increased (pH 13), the oxygen-related groups were dramatically enhanced (see Table S1) in comparison to pristine material (pH 8). In addition, the high pH led to the transformation of carbonyl groups into carboxyl groups due to the deprotonation effect (see Table S2). However, the low pH (3) created lower carbonyl and carboxyl groups (Table S1) with relatively higher carbonyl content (Table S2) showing the protonation effect. In a similar vein, conversely to oxygen-related groups, the pyrrolic form of N was remarkably enhanced with protonation and decreased with deprotonation (Table S3). With the increase in the ratio of positively-charged N-H groups, CQDs lost their high negative surface charge, became more unstable and finally, aggregation was observed accordingly. Considering all the data presented so far, under the alkaline conditions, a red shift in PL emission was observed, similar to other studies in the literature [39–43], indicating the emergence of a negative ‘protective shell’ due to the deprotonation. However, the low pH remarkably altered surface functional groups, zeta potential, and finally, aggregation-induced PL emission.

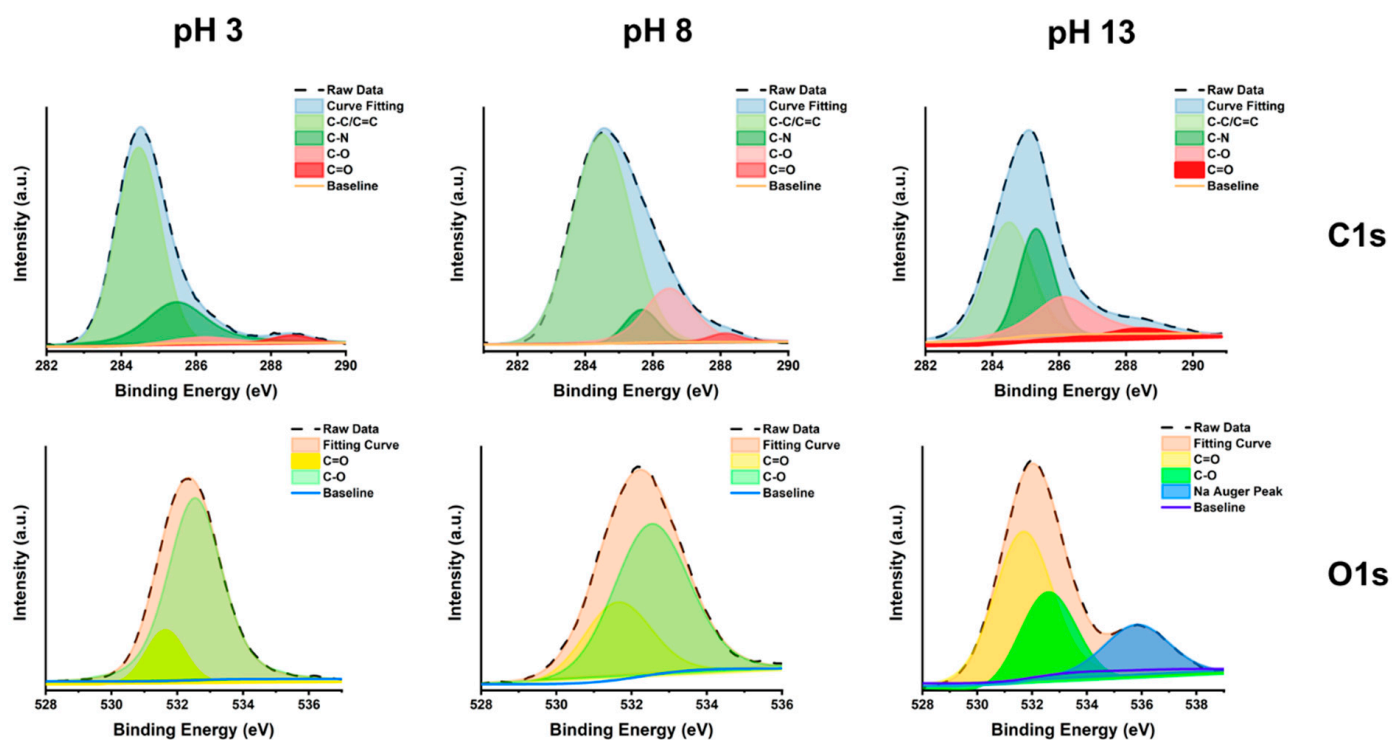
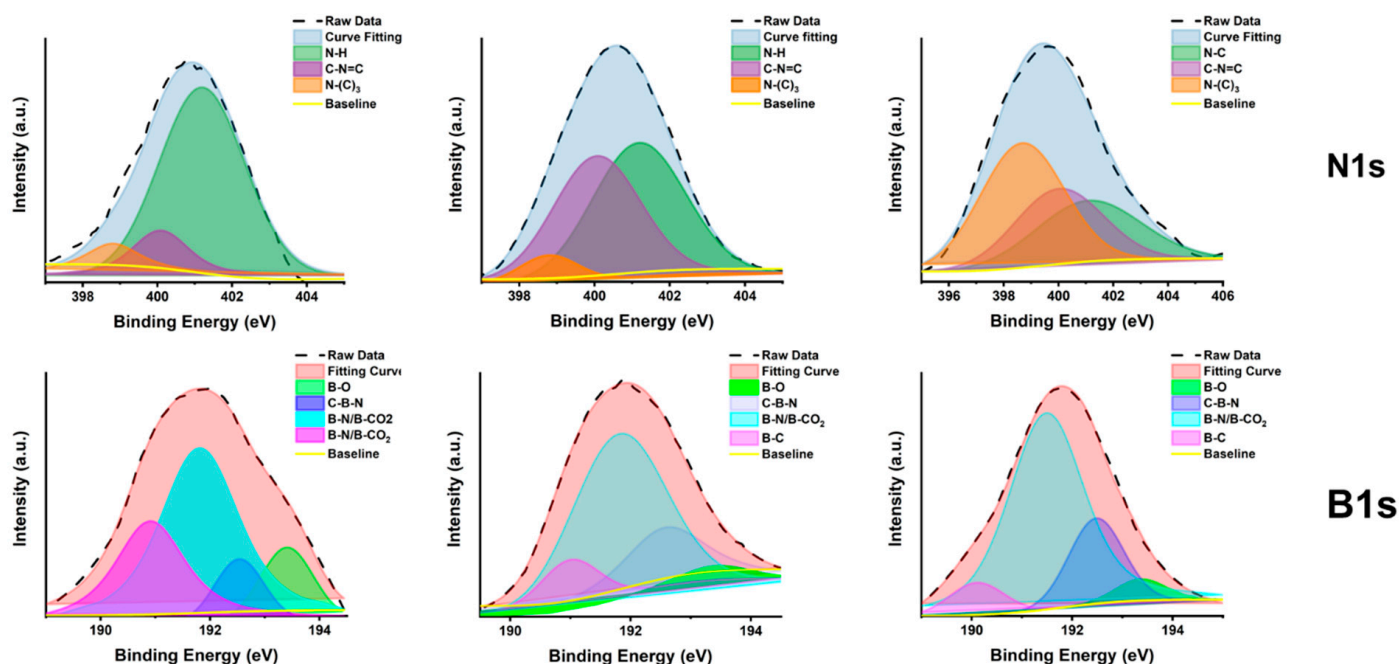


Figure 3. Cont.



**Figure 3.** High-resolution XPS spectra of high-resolution C1s, O1s, N1s, and B1s at different pH conditions.

#### 4. Conclusions

In summary, we have synthesized B/N-CQDs via a facile hydrothermal procedure using dopamine and sodium borohydride as precursors with a high QY and excitation-dependent nature. The PL characteristics of the CQDs were manipulated by simply tuning the pH of the medium. Under acidic conditions, B/N-CQDs exhibited strong green fluorescence emission with the loss of the excitation-dependent nature. This unique alteration was attributed to the protonation of surface groups, decrease in negative surface charge, and finally, aggregation of the nanostructure. However, in the case of alkaline conditions, the deprotonation surface groups significantly enhanced the surface charge and led to the emergence of a negative ‘protective shell’. PL spectra showed the loss of excitation-dependent features and led to a red-shift in emission peak maxima with lower intensity. This report obviously demonstrates that the proposed CQDs might provide unique advantages in novel pH sensor systems and fluorescence imaging where a pH-sensitive fluorescence activity is demanded in a wide range of pH conditions. The findings provided in this study clarify the pH-sensitive PL mechanism of CQDs. The practical applications are pH monitoring inside cells, control, and monitoring pH-active drugs, and bioimaging.

**Supplementary Materials:** The following supporting information can be downloaded at: <https://www.mdpi.com/article/10.3390/coatings13020456/s1>, Figure S1: The PL spectra of B/N-CQDs at different pH conditions and excitation wavelengths; Figure S2: Optic images of CQDs at different pH conditions under a 365-nm UV lamp (a) and daylight (b); Figure S3: UV-vis absorption spectra of B/N-CQDs at different pH; Figure S4: XPS survey spectrum (a) and elemental percentage of B/N-CQDs (b) under different pH conditions; Table S1: Deconvolution of C1s under different pH conditions; Table S2: Deconvolution of O1s under different pH conditions; Table S3: Deconvolution N1s under different pH conditions.

**Author Contributions:** Conceptualization, O.U., S.N.K. and M.Y.; methodology, O.U., S.N.K. and M.Y.; software, O.U., H.M., A.Y. and M.Y.; validation O.U., H.M., A.Y. and M.Y.; formal analysis, A.Y. and M.Y.; investigation, O.U., H.M., A.Y. and M.Y.; resources, O.U., A.Y. and M.Y.; data curation, O.U. and M.Y.; writing—original draft preparation, O.U., A.Y. and M.Y.; writing—review and editing, O.U., H.M., A.Y. and M.Y.; visualization, A.Y. and M.Y.; supervision A.Y. and M.Y.; project administration, A.Y. and M.Y.; funding acquisition, A.Y. and M.Y. All authors have read and agreed to the published version of the manuscript.

**Funding:** This work was supported by Ataturk University Scientific Research Project Coordination Unit (AU-BAP, No.: FAB-2021-9302).

**Institutional Review Board Statement:** Not applicable.

**Informed Consent Statement:** Not applicable.

**Data Availability Statement:** Not applicable.

**Acknowledgments:** The authors also kindly acknowledge the East Anatolia High Technology Application and Research Center (DAYTAM) at Ataturk University for providing laboratory spaces and characterization devices.

**Conflicts of Interest:** The authors declare no conflict of interest.

## References

1. Aydin, S.; Ustun, O.; Ghosigharehaghaji, A.; Tavaci, T.; Yilmaz, A.; Yilmaz, M. Hydrothermal Synthesis of Nitrogen-Doped and Excitation-Dependent Carbon Quantum Dots for Selective Detection of Fe<sup>3+</sup> in Blood Plasma. *Coatings* **2022**, *12*, 1311. [\[CrossRef\]](#)
2. John, B.K.; Abraham, T.; Mathew, B. A Review on Characterization Techniques for Carbon Quantum Dots and Their Applications in Agrochemical Residue Detection. *J. Fluoresc.* **2022**, *32*, 449–471. [\[CrossRef\]](#)
3. Karadag, S.N.; Ustun, O.; Yilmaz, A.; Yilmaz, M. The Fabrication of Excitation-Dependent Fluorescence Boron/Nitrogen Co-Doped Carbon Quantum Dots and Their Employment in Bioimaging. *Chem. Phys.* **2022**, *562*, 111678. [\[CrossRef\]](#)
4. Malavika, J.P.; Shobana, C.; Sundarraj, S.; Ganeshbabu, M.; Kumar, P.; Selvan, R.K. Green Synthesis of Multifunctional Carbon Quantum Dots: An Approach in Cancer Theranostics. *Biomater. Adv.* **2022**, *136*, 212756. [\[CrossRef\]](#)
5. Hu, X.; Han, W.; Zhang, M.; Li, D.; Sun, H. Enhanced Adsorption and Visible-Light Photocatalysis on TiO<sub>2</sub> with in situ Formed Carbon Quantum Dots. *Environ. Sci. Pollut. Res.* **2022**, *29*, 56379–56392. [\[CrossRef\]](#)
6. Dhandapani, E.; Sengodan, P.; Duraisamy, N.; Ramesh, R. Fabrication of Semi-Flexible Carbon Quantum Dots-Reinforced Polypyrrole (PPy/CQDs) Composite Electrodes by Hybrid Electrospray Deposition for High-Performance Energy Storage Device. *Int. J. Energy Res.* **2022**, *46*, 7277–7292. [\[CrossRef\]](#)
7. Behi, M.; Gholami, L.; Naficy, S.; Palomba, S.; Dehghani, F. Carbon Dots: A Novel Platform for Biomedical Applications. *Nanoscale Adv.* **2022**, *4*, 353–376. [\[CrossRef\]](#)
8. Eivazzadeh-keihan, R.; Noruzi, E.B.; Chidar, E.; Jafari, M.; Davoodi, F.; Kashtiaray, A.; Gorab, M.G.; Hashemi, S.M.; Javanshir, S.; Cohan, R.A.; et al. *Applications of Carbon-Based Conductive Nanomaterials in Biosensors*; Elsevier B.V.: Amsterdam, The Netherlands, 2022; ISBN 9821732283.
9. Şen, F.B.; Beğiç, N.; Bener, M.; Apak, R. Fluorescence Turn-off Sensing of TNT by Polyethylenimine Capped Carbon Quantum Dots. *Spectrochim. Acta—Part A Mol. Biomol. Spectrosc.* **2022**, *271*, 120884. [\[CrossRef\]](#)
10. Liu, C.; Zhang, F.; Hu, J.; Gao, W.; Zhang, M. A Mini Review on PH-Sensitive Photoluminescence in Carbon Nanodots. *Front. Chem.* **2021**, *8*, 605028. [\[CrossRef\]](#)
11. Ding, H.; Li, X.H.; Chen, X.B.; Wei, J.S.; Li, X.B.; Xiong, H.M. Surface States of Carbon Dots and Their Influences on Luminescence. *J. Appl. Phys.* **2020**, *127*, 231101. [\[CrossRef\]](#)
12. Zhu, S.; Song, Y.; Zhao, X.; Shao, J.; Zhang, J.; Yang, B. The Photoluminescence Mechanism in Carbon Dots (Graphene Quantum Dots, Carbon Nanodots, and Polymer Dots): Current State and Future Perspective. *Nano Res.* **2015**, *8*, 355–381. [\[CrossRef\]](#)
13. Lim, S.Y.; Shen, W.; Gao, Z. Carbon Quantum Dots and Their Applications. *Chem. Soc. Rev.* **2015**, *44*, 362–381. [\[CrossRef\]](#)
14. Ehtesabi, H.; Hallaji, Z.; Najafi Nobar, S.; Bagheri, Z. Carbon Dots with PH-Responsive Fluorescence: A Review on Synthesis and Cell Biological Applications. *Microchim. Acta* **2020**, *187*, 150. [\[CrossRef\]](#)
15. Rahmani, E.; Pourmadadi, M.; Ghorbanian, S.A.; Yazdian, F.; Rashedi, H.; Navaee, M. Preparation of a PH-Responsive Chitosan-Montmorillonite-Nitrogen-Doped Carbon Quantum Dots Nanocarrier for Attenuating Doxorubicin Limitations in Cancer Therapy. *Eng. Life Sci.* **2022**, *22*, 634–649. [\[CrossRef\]](#)
16. Yang, Y.Z.; Xiao, N.; Liu, S.G.; Han, L.; Li, N.B.; Luo, H.Q. PH-Induced Aggregation of Hydrophilic Carbon Dots for Fluorescence Detection of Acidic Amino Acid and Intracellular PH Imaging. *Mater. Sci. Eng. C* **2020**, *108*, 110401. [\[CrossRef\]](#)
17. Wang, X.; Zhao, L.; Hu, J.; Wei, H.; Liu, X.; Li, E.; Yang, S. Rational Design of Novel Carbon-Oxygen Quantum Dots for Ratiometrically Mapping PH and Reactive Oxygen Species Scavenging. *Carbon N. Y.* **2022**, *190*, 115–124. [\[CrossRef\]](#)
18. Liu, H.; Ye, T.; Mao, C. Fluorescent Carbon Nanoparticles Derived from Candle Soot. *Angew. Chemie* **2007**, *119*, 6593–6595. [\[CrossRef\]](#)
19. Lu, S.; Cong, R.; Zhu, S.; Zhao, X.; Liu, J.; Tse, J.S.; Meng, S.; Yang, B. PH-Dependent Synthesis of Novel Structure-Controllable Polymer-Carbon NanoDots with High Acidophilic Luminescence and Super Carbon Dots Assembly for White Light-Emitting Diodes. *ACS Appl. Mater. Interfaces* **2016**, *8*, 4062–4068. [\[CrossRef\]](#)
20. Zhu, J.; Chu, H.; Shen, J.; Wang, C.; Wei, Y. Carbon Quantum Dots with PH-Responsive Orange-/Red-Light Emission for Fluorescence Imaging of Intracellular PH. *Microchim. Acta* **2023**, *190*, 21. [\[CrossRef\]](#)
21. Fan, X.; Wang, Y.; Li, B.; Shen, C.; Sun, Z.; Zhan, Y.; Zhang, Y. Highly Luminescent PH-Responsive Carbon Quantum Dots for Cell Imaging. *Nanotechnology* **2022**, *33*, 265002. [\[CrossRef\]](#)

22. Li, C.; Zhang, X.; Zhang, W.; Qin, X.; Zhu, C. Carbon Quantum Dots Derived from Pure Solvent Tetrahydrofuran as a Fluorescent Probe to Detect PH and Silver Ion. *J. Photochem. Photobiol. A Chem.* **2019**, *382*, 111981. [[CrossRef](#)]
23. Wang, L.; Li, M.; Li, W.; Han, Y.; Liu, Y.; Li, Z.; Zhang, B.; Pan, D. Rationally Designed Efficient Dual-Mode Colorimetric/Fluorescence Sensor Based on Carbon Dots for Detection of PH and Cu<sup>2+</sup> Ions. *ACS Sustain. Chem. Eng.* **2018**, *6*, 12668–12674. [[CrossRef](#)]
24. Sun, Y.; Wang, X.; Wang, C.; Tong, D.; Wu, Q.; Jiang, K.; Jiang, Y.; Wang, C.; Yang, M. Red Emitting and Highly Stable Carbon Dots with Dual Response to PH Values and Ferric Ions. *Microchim. Acta* **2018**, *185*, 83. [[CrossRef](#)]
25. Ye, X.; Xiang, Y.; Wang, Q.; Li, Z.; Liu, Z. A Red Emissive Two-Photon Fluorescence Probe Based on Carbon Dots for Intracellular PH Detection. *Small* **2019**, *15*, e1901673. [[CrossRef](#)]
26. Choi, Y.; Kang, B.; Lee, J.; Kim, S.; Kim, G.T.; Kang, H.; Lee, B.R.; Kim, H.; Shim, S.H.; Lee, G.; et al. Integrative Approach toward Uncovering the Origin of Photoluminescence in Dual Heteroatom-Doped Carbon Nanodots. *Chem. Mater.* **2016**, *28*, 6840–6847. [[CrossRef](#)]
27. Das, S.K.; Liu, Y.; Yeom, S.; Kim, D.Y.; Richards, C.I. Single-Particle Fluorescence Intensity Fluctuations of Carbon Nanodots. *Nano Lett.* **2014**, *14*, 620–625. [[CrossRef](#)]
28. Wang, W.; Lu, Y.C.; Huang, H.; Feng, J.J.; Chen, J.R.; Wang, A.J. Facile Synthesis of Water-Soluble and Biocompatible Fluorescent Nitrogen-Doped Carbon Dots for Cell Imaging. *Analyst* **2014**, *139*, 1692–1696. [[CrossRef](#)]
29. Wang, H.; Sun, P.; Cong, S.; Wu, J.; Gao, L.; Wang, Y.; Dai, X.; Yi, Q.; Zou, G. Nitrogen-Doped Carbon Dots for “Green” Quantum Dot Solar Cells. *Nanoscale Res. Lett.* **2016**, *11*, 1–6. [[CrossRef](#)]
30. Richardson, I.E.G. Front Matter and Index. In *Video Codec Design*; John Wiley & Sons: Hoboken, NJ, USA, 2003; pp. i–x.
31. Lakowicz, J.R. *Principles of Fluorescence Spectroscopy*; Springer: Boston, MA, USA, 2006; ISBN 0387312781.
32. Ye, R.; Xiang, C.; Lin, J.; Peng, Z.; Huang, K.; Yan, Z.; Cook, N.P.; Samuel, E.L.G.; Hwang, C.C.; Ruan, G.; et al. Coal as an Abundant Source of Graphene Quantum Dots. *Nat. Commun.* **2013**, *4*, 2943. [[CrossRef](#)]
33. Jia, X.; Yang, X.; Li, J.; Li, D.; Wang, E. Stable Cu Nanoclusters: From an Aggregation-Induced Emission Mechanism to Biosensing and Catalytic Applications. *Chem. Commun.* **2014**, *50*, 237–239. [[CrossRef](#)]
34. Su, Y.; Xie, Z.; Zheng, M. Carbon Dots with Concentration-Modulated Fluorescence: Aggregation-Induced Multicolor Emission. *J. Colloid Interface Sci.* **2020**, *573*, 241–249. [[CrossRef](#)]
35. Keerthana, P.; Cherian, A.R.; Sirimahachai, U.; Thadathil, D.A.; Varghese, A.; Hegde, G. Detection of Picric Acid in Industrial Effluents Using Multifunctional Green Fluorescent B/N-Carbon Quantum Dots. *J. Environ. Chem. Eng.* **2022**, *10*, 107209. [[CrossRef](#)]
36. Mohammed, L.J.; Omer, K.M. Dual Functional Highly Luminescence B, N Co-Doped Carbon Nanodots as Nanothermometer and Fe<sup>3+</sup>/Fe<sup>2+</sup> Sensor. *Sci. Rep.* **2020**, *10*, 3028. [[CrossRef](#)]
37. Wei, Y.; Chen, L.; Wang, J.; Liu, X.; Yang, Y.; Yu, S. Investigation on the Chirality Mechanism of Chiral Carbon Quantum Dots Derived from Tryptophan. *RSC Adv.* **2019**, *9*, 3208–3214. [[CrossRef](#)]
38. Mutuma, B.K.; Matsoso, B.J.; Momodu, D.; Oyedotun, K.O.; Coville, N.J.; Manyala, N. Deciphering the Structural, Textural, and Electrochemical Properties of Activated BN-Doped Spherical Carbons. *Nanomaterials* **2019**, *9*, 446. [[CrossRef](#)]
39. Li, S.; Song, X.; Wang, Y.; Hu, Z.; Yan, F.; Feng, G. Developed a Ratiometric Fluorescence PH Nanosensor Based on Label-Free Carbon Dots for Intracellular Lysosome Imaging and Water PH Monitoring with a Smartphone. *Dye. Pigment.* **2021**, *193*, 109490. [[CrossRef](#)]
40. Song, Z.; Quan, F.; Xu, Y.; Liu, M.; Cui, L.; Liu, J. Multifunctional N,S Co-Doped Carbon Quantum Dots with PH- and Thermo-Dependent Switchable Fluorescent Properties and Highly Selective Detection of Glutathione. *Carbon N. Y.* **2016**, *104*, 169–178. [[CrossRef](#)]
41. Lei, C.W.; Hsieh, M.L.; Liu, W.R. A Facile Approach to Synthesize Carbon Quantum Dots with PH-Dependent Properties. *Dye. Pigment.* **2019**, *169*, 73–80. [[CrossRef](#)]
42. Yu, J.; Liu, C.; Yuan, K.; Lu, Z.; Cheng, Y.; Li, L.; Zhang, X.; Jin, P.; Meng, F.; Liu, H. Luminescence Mechanism of Carbon Dots by Tailoring Functional Groups for Sensing Fe<sup>3+</sup> Ions. *Nanomaterials* **2018**, *8*, 233. [[CrossRef](#)]
43. Dai, X.; Wang, H.; Qian, Z.; Yi, Q.; Wang, Y.; Cong, S.; Zhao, J.; Sun, Y.; Huang, J.; Xiong, J.; et al. Emission Switching in Carbon Dots Coated CdTe Quantum Dots Driving by PH Dependent Hetero-Interactions. *Appl. Phys. Lett.* **2015**, *107*, 203108. [[CrossRef](#)]

**Disclaimer/Publisher’s Note:** The statements, opinions and data contained in all publications are solely those of the individual author(s) and contributor(s) and not of MDPI and/or the editor(s). MDPI and/or the editor(s) disclaim responsibility for any injury to people or property resulting from any ideas, methods, instructions or products referred to in the content.